

UWB Compact Microstrip Patch Antenna with High Directivity Using Novel Star-Shaped Frequency Selective Surface

Rajesh Kumar^{1, *} and Devi C. Dhubkarya²

Abstract—This paper presents a single element ultra-wideband (UWB) microstrip patch antenna with high directivity. In this work, techniques like partial ground and modification of the patch have been used to achieve the UWB. The designed antenna consists of a modified U-shaped radiating patch with a microstrip feed attached directly to it. The initial U-shaped radiating patch is modified by attaching an inverted trapezium on both sides of the feed line. Two parasitic patches are introduced near the feed structure of the antenna after etching away two rectangular slots with appropriate dimensions. Moreover, the proposed structure consists of a partial ground plane which contributes to the UWB nature. Modifications in the form of square and triangular slot etching are carried out in this part of the proposed structure. The proposed antenna is compact with dimensions of $16\text{ mm} \times 19\text{ mm} \times 1.6\text{ mm}$. Finally, gain enhancement of the proposed structure is done by placing a Frequency Selective Surface (FSS) behind the proposed antenna with an air spacer in between the structures. A novel FSS unit cell is proposed, and its performances are checked experimentally. Later, FSS is combined with the antenna, and measured peak gain of 9.7 dBi is obtained experimentally. The overall size of the structure is $62.5\text{ mm} \times 52\text{ mm} \times 24.9\text{ mm}$.

1. INTRODUCTION

Ultra-wideband (UWB) represents the frequency range from 3.1 to 10.6 GHz given by the Federal Communications Commission (FCC), having a fractional bandwidth of 110%. UWB antennas have numerous applications due to their high bandwidth, low energy requirement and less multipath fading [1]. These systems need antennas having a large bandwidth [2] to make the system competitive with other communication systems. UWB antennas with compact size, wide impedance bandwidth, and highly directional radiation pattern are in huge demand. They are also utilized for monostatic and multi-static radar imaging for target tracking and target data retrieval [3, 4]. Low gain and bidirectional radiation pattern are the limitations of a conventional UWB antenna. A metallic reflector can be used to improve the gain, but the overall RCS increases. In order to address this issue, frequency selective surface (FSS) is introduced which improves the gain at selective frequencies.

FSSs are two dimensional periodic arrays of symmetric unit cells printed on a dielectric substrate without any ground plane [5]. Owing to their diverse merits, several researchers are currently working to design and develop application specific FSSs for various modern day applications documented in [6–19]. A compact, low profile, dual polarized UWB FSS is proposed in [12], where the FSS is designed using two similar metallic array structures separated by dielectric material. A novel UWB FSS based polarization diversity antenna is explained in [13], which consists of a dual polarized radiator mounted on a backing reflector made up of a single layer FSS. The design produced an average gain of 9.5 dBi. [14] discusses a novel FSS exploiting miniaturized hexagonal rings, where a UWB stopband and an

Received 3 March 2022, Accepted 31 March 2022, Scheduled 22 April 2022

* Corresponding author: Rajesh Kumar (heyrajeshkumar@yahoo.com).

¹ Department of ECE, Sachdeva Institute of Technology, Mathura, UP, India. ² Department of ECE, Bundelkhand Institute of Engineering & Technology, Jhansi, UP, India.

improved polarization independence property are achieved due to the compact arrangement of the hexagonal rings. A compact unilayer FSS to enhance the gain of an UWB monopole antenna is presented in [15], where the FSS unit cells are composed of simple metallic patterns printed on both sides of the substrate. The gain of the antenna is improved by 4 dBi after the FSS installation. A compact coplanar waveguide (CPW) fed UWB antenna with bended ground plane suitable for ground penetrating radar (GPR) applications is proposed in [16, 17]. Here, a double layered FSS structure is incorporated with the antenna to get an overall gain improvement around 2 to 4 dBi. A highly compact UWB monopole antenna with a peak gain of 9.4 dBi is elaborated in [18]. Finally, an ultra-wide stopband single-layer FSS with high incident angle independence has been proposed in [19], which consists of four asymmetric rectangular patches with circular slots embedded in it.

Recently, UWB antennas integrated with FSS is utilized for GPR and microwave imaging applications. GPR is a subsurface scanning device that uses UWB antenna for transmission and reception of electromagnetic waves to produce a 3-D image of the subsurface from the backscattered wave [20]. Various FSS designs for GPR applications are elaborated in [21–24]. Microwave imaging is a popular method of obtaining the internal images of objects without breaking apart the Materials Under Test (MUT). Varieties of FSS based high gain antennas are necessary in the current scenario to obtain a very good information about the target, and they are elaborated in [25–27].

Conventional UWB antenna structures that are reported include — triangular [28], rectangular [29], elliptical [30, 31], circular [32], semi-elliptical [33], U-shaped [34, 35], etc. Defected ground plane and addition of slots [36] are common techniques to introduce UWB behavior. Various compact UWB antennas are discussed in [37–39]. Among the UWB antennas developed, planar monopole antenna [40–44] has attracted the most attention since it can be integrated with other devices perfectly.

Practical applications like high-accuracy positioning systems, portable devices, microwave imaging, and GPR applications demand a highly directive antenna with a stable radiation pattern and high gain [45]. Different gain enhancement techniques have been reported in literature such as the introduction of gate-like metallic structures [46], electromagnetic band gap (EBG) [47], and using dielectric resonator antenna (DRA) [48]. Using different feeding techniques [49], or by increasing the number of layers in the antenna array [50], the antenna gain can be improved further. The most common method by which the Frequency Selective Surface is employed is a reflector. The FSS is kept behind the antenna, and the distance to the antenna is optimized in such a way that it reflects the radiation in the desired direction [51–53].

In this work, an FSS of dimensions $52 \times 62.5 \times 1.6 \text{ mm}^3$ is designed first followed by the UWB antenna of dimensions $18 \times 16 \times 1.6 \text{ mm}^3$. The designed FSS shifts the peak gain of the proposed antenna by more than 6 dBi, and also the UWB characteristics of the antenna are also improved. The proposed antenna can be used in a wide range of applications like GPRs, microwave imaging, etc.

2. PROPOSED GEOMETRY AND DESCRIPTION

2.1. Design of Frequency Selective Surface (FSS)

FSS is a two dimensional periodic array of symmetric unit cells on a dielectric substrate without any ground plane [5]. FSS can be thought as the wireless counterpart of conventional filters that are used in electronic circuits as it provides spatial filtering characteristics. Patch type FSS exhibits the response of a band stop filter, and aperture type FSS behaves like a band pass filter when the unit cell dimension is compatible to the wavelength corresponding to the resonating frequency. The schematic view of the FSS unit cell is shown in Fig. 1(a). A single element FSS unit cell is simulated in CST Microwave Studio 2014 using periodic boundary conditions. The proposed FSS consists of a star-shaped structure inside a circular slot. The periodicity of the proposed FSS is 10.5 mm, and it is on an FR-4 substrate with dielectric constant 4.4 and loss tangent 0.02. The dimensions of the proposed FSS array are $52 \times 62.5 \times 1.6 \text{ mm}^3$. The schematic of the complete FSS structure is depicted in Fig. 1(b). The proposed FSS shows a wide stopband for $S_{21} < -15 \text{ dB}$ over 8–12 GHz. The simulated filtering characteristics of the proposed FSS unit cell is shown in Fig. 2(a). The FSS is modelled as a series RLC, and the equivalent circuit model is shown in Fig. 2(b) for better clarity. The modelled equivalent circuit is then utilized to find the R , L and C values. The stopband of the FSS is noted, and then the obtained value is exported to Advanced Design Systems (ADS) software. The weights of R , L , and C

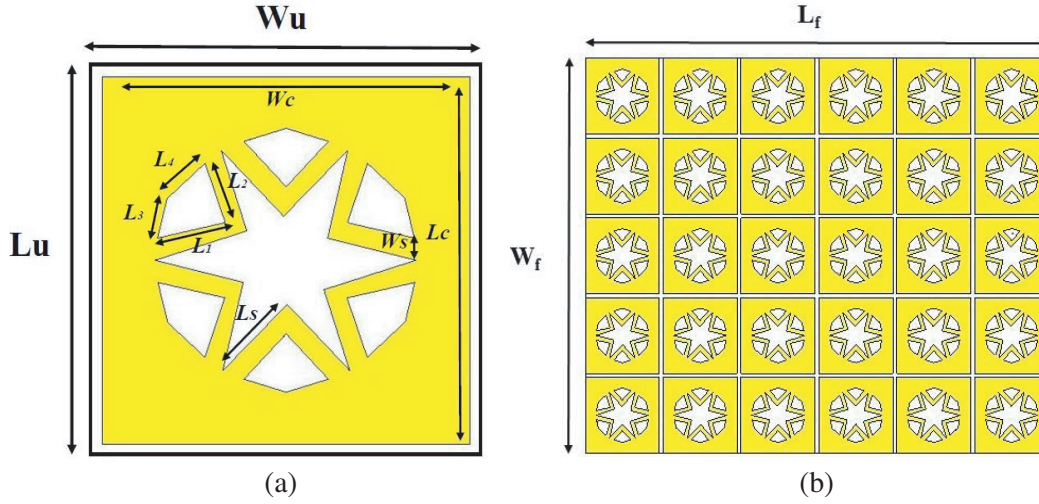


Figure 1. (a) Schematic view of the proposed FSS unit cell unitcell, and (b) proposed FSS structure where $L_f = 62.5$ mm and $W_f = 52$ mm.

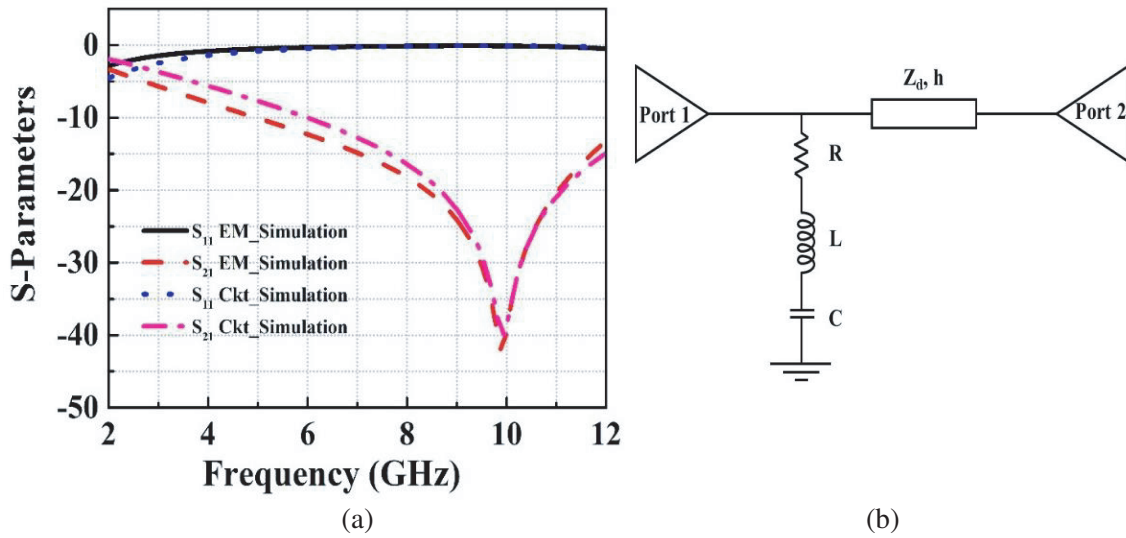


Figure 2. (a) Simulated filtering characteristics of the proposed FSS unit cell, and (b) the equivalent circuit model of the proposed FSS unit cell.

are simultaneously changed such that the new result matches the curve obtained from the EM simulator. Thus, the values of R , L , and C are obtained as 1.57Ω , 1.0087 nH, and 0.2548 pF, respectively. The input impedance of the FSS for the equivalent circuit is obtained by Eq. (1)

$$Z_s = R + j \left(L - \frac{1}{C} \right) \tag{1}$$

Transmission matrix ($ABCD$ parameter) of the FSS cascaded with the dielectric substrate can be found using Eq. (2),

$$\begin{bmatrix} A & B \\ C & D \end{bmatrix} = \begin{bmatrix} 1 & 0 \\ \frac{1}{Z_s} & 1 \end{bmatrix} \begin{bmatrix} \cos \beta h & jZ_d \sin \beta h \\ j\frac{1}{Z_d} \sin \beta h & \cos \beta h \end{bmatrix} = \begin{bmatrix} \cos \beta h & jZ_d \sin \beta h \\ \frac{\cos \beta h}{Z_s} + j\frac{1}{Z_d} \sin \beta h & \cos \beta h + j\frac{Z_d}{Z_s} \sin \beta h \end{bmatrix} \tag{2}$$

The relation between the $ABCD$ parameter and reflection (R) and transmission (T) coefficient are given by Eqs. (3)–(4)

$$R = \frac{A + \frac{B}{Z_0} - CZ_0 - D}{A + \frac{B}{Z_0} + CZ_0 + D} \quad (3)$$

$$T = \frac{2}{A + \frac{B}{Z_0} + CZ_0 + D} \quad (4)$$

where A , B , C , and D are the $ABCD$ network parameters; Z_0 represents the characteristic impedance; ϵ_r is the dielectric constant; β is the phase constant; h is the substrate thickness, and $Z_d = \frac{Z_0}{\sqrt{\epsilon_r}}$. Eqs. (1)–(4) are utilized to find the reflection and transmission coefficients as represented by R and T , respectively. Once the R , L , C values are obtained from ADS, the following values can be used in Eqs. (1)–(4) to obtain R and T from MATLAB. These equations are a generalized method of finding the reflection and transmission coefficients once the parameters are obtained from ADS.

2.2. Design of an UWB Antenna

The detailed description of the geometry of the proposed structure is shown in Fig. 3. The basic design consists of a radiating patch on top of a substrate with a thickness of h . The dimensions of the substrate are given by $L_{\text{sub}} \times W_{\text{sub}} \times h$. The patch is made up of a modified U-shaped radiating patch. The initial radius of the U-shaped patch is given by R_u . This part is then extended by connecting a rectangular section of dimension $L_{\text{rect}} \times W_{\text{rect}}$ as an extension to the U-shaped radiator. A trapezium of sides L_{t1} , L_{t2} , L_{t3} , with the base extending from the junction of the microstrip feed and U-shaped patch to the starting point of the U-shaped arc is attached on the two sides of the initial radiator to get the modified U-shaped patch antenna. The modified U shape is now ready. The modified U shape is then connected to a microstrip patch of length L_m and width W_m . The width of the microstrip feeding input W_m is taken as 3 mm to match the 50Ω characteristic impedance. Finally, two rectangular slots of dimension $L_{\text{slot}} \times W_{\text{slot}}$ on opposite sides of the feed line are etched out, and two parasitic patches are kept near the

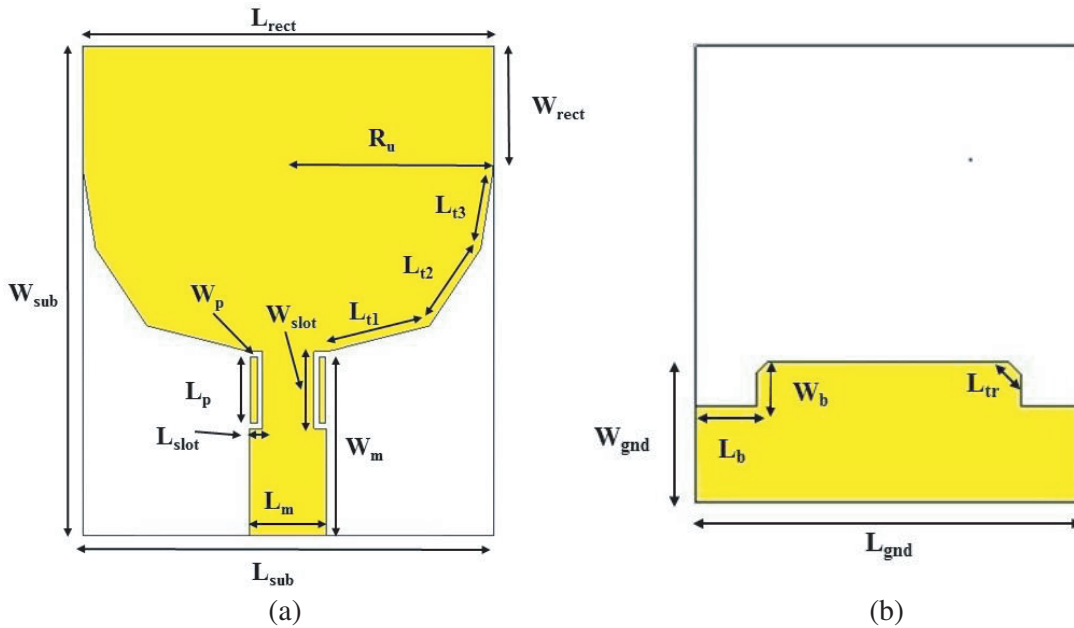


Figure 3. Detailed geometry of the proposed UWB antenna where (a) front side and (b) back side.

etched-out region on opposite sides at a distance d from the etched out region of the microstrip feed line. The dimension of the parasitic patch is given by $L_p \times W_p$. For designing the antenna, an inexpensive FR-4 epoxy substrate is used with relative dielectric constant (ϵ_r) of 4.4 and loss tangent ($\tan \delta$) of 0.02. On the back side of the substrate, a rectangular conducting ground plane is created with dimensions of $L_{\text{gnd}} \times W_{\text{gnd}}$. To achieve UWB characteristics, modifications on the ground plane have been done. A slot of dimension $L_b \times W_b$ on both sides of the ground patch on the upper side of the patch edge is removed. A small triangle of side L_{tr} is etched out from the rectangular edges to complete the antenna design. To further improve the gain and directivity, a frequency selective surface (FSS) with dimensions $L_f \times W_f \times h$ is placed behind the proposed antenna with an air spacer in between them, completing the entire design of the proposed structure. The optimized dimensions of the designed antenna are given in in Table 1.

Table 1. All structural dimensions of the proposed antenna.

	Parameters	Dimension (mm)	Parameters	Dimension (mm)	Parameters	Dimension (mm)
Substrate	L_{sub}	16	W_{sub}	19	h	1.6
Patch	L_{rect}	16	W_{rect}	4	R_u	8
Trapezium (sides)	L_{t1}	4.65	L_{t2}	3.6	L_{t3}	3
Stripline (Feed)	L_m	3	W_m	7.2	-	-
Ground	L_{gnd}	16	W_{gnd}	6	-	-
Slots (Patch)	L_{slot}	0.5	W_{slot}	3	-	-
Slots (Ground)	L_b	2.5	W_b	2	L_{tr}	0.7 mm
Parasitic Patch	L_p	0.25	W_p	2.6	-	-
Proposed FSS	L_f	62.5	W_f	52	h	1.6
Distance between Antenna and FSS	L_{af}	20				

The UWB characteristics can be achieved by modifying the ground plane. The various stages in the design of the proposed antenna are elaborated in Fig. 4. The primary antenna is a U-shaped antenna with a rectangular ground plane as shown in Fig. 4(a). Two trapeziums having the side lengths mentioned above are added to this antenna in order to get the modified U-shaped patch antenna in Fig. 4(b). To further improve the matching, two rectangular slots are embedded in the ground plane of the above modified structure to get a better impedance bandwidth, as shown in Fig. 4(c). Then, a slot is made in the microstrip feed line, and two rectangular patches are made near the above two slots. A small triangle-shaped patch is then etched out of the rectangular pointing edges in the ground plane to get the final design as shown in Fig. 4(d). The operational bandwidth of the antenna is increased by the modifications made on the ground plane as well as due to the addition of the parasitic patches near the feeding portion of the proposed antenna. The return losses at different stages leading up to the final proposed antenna are shown in Fig. 5. Finally, the FSS is incorporated at a distance L_f behind the UWB, and its position with respect to antenna is adjusted in such a way that good impedance match

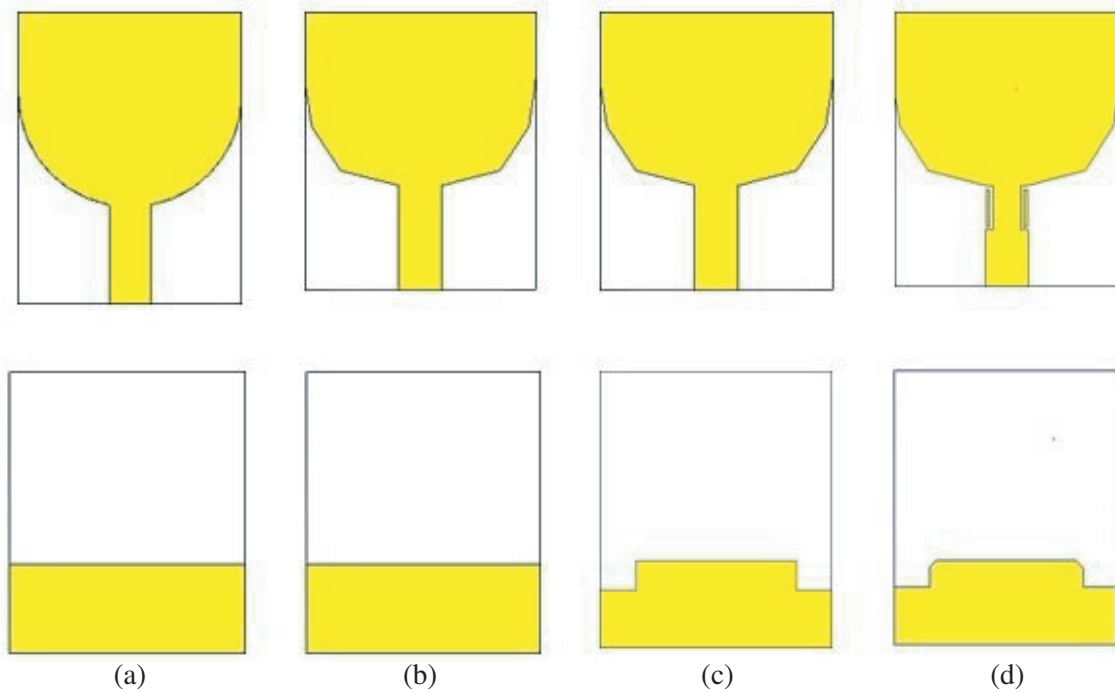


Figure 4. Design stages in the development of the final single element UWB microstrip patch antenna. (a) Stage_1. (b) Stage_2. (c) Stage_3. (d) Stage_4.

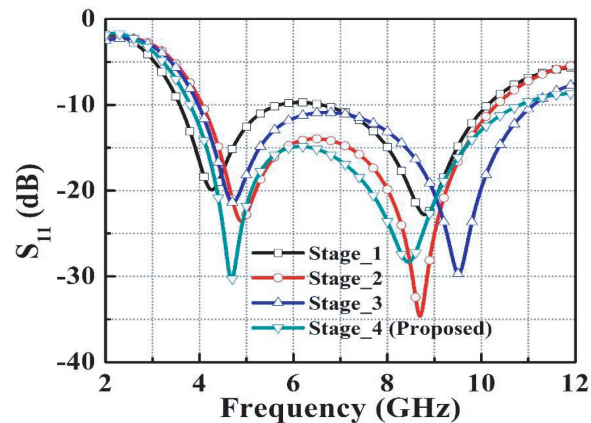


Figure 5. Simulated return loss responses at different design stages of the antenna where stage-4 is chosen as the final design.

as well as good gain is obtained. Fig. 6(a) shows the arrangement of the FSS behind the UWB antenna, and the perspective view of the complete structure is shown in Fig. 6(b). The final optimized operational bandwidth achieved by the combination of antenna and the FSS is from 3.6 GHz to 10.8 GHz.

3. SIMULATED RESPONSES OF THE ANTENNA COMBINED WITH THE FSS

A single element UWB antenna with high directivity is designed using the patch and partial etching of the ground plane. A compact antenna is designed over the UWB range (3.6 GHz to 10.8 GHz) in CST Microwave Studio Suite 2014. Instead of the SMA connector used practically, waveguide port is used in the simulator.

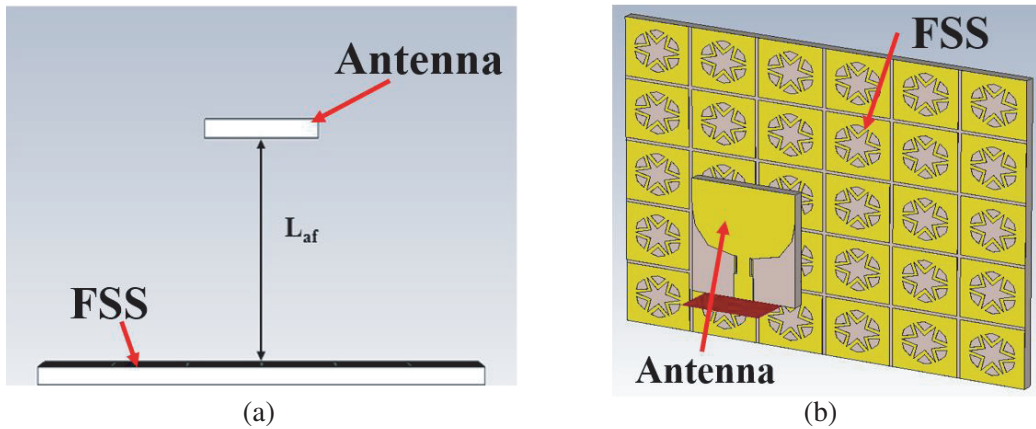


Figure 6. (a) The relative position of the FSS as compared to the UWB antenna, and (b) perspective view of the complete structure.

An extensive full-wave simulation is carried out to understand the different parameters related to the proposed antenna and to study its diverse performances. The impedance bandwidth or return loss and gain are obtained initially without the FSS. Finally, the radiation characteristics of the proposed antenna are studied and then plotted with and without the FSS. The proposed structure is simulated with and without the FSS. The overall simulated impedance bandwidth is better in the case of the antenna with FSS. When the antenna alone is excited, the impedance bandwidth is from 3.6 GHz to about 10.8 GHz. Design of the antenna is varied in such a way that the impedance bandwidth obtained is in the UWB range. After this step, the FSS is loaded behind the antenna at a distance of L_{af} , and the impedance bandwidth is again checked. The -10 dB return losses of the proposed UWB antenna with and without the FSS integration are simulated and studied in Fig. 7. The results show that the FSS with antenna gives much better response than the stand alone UWB structure. An extra resonance is formed after the addition of the FSS. This is due to the resonance of the cavity formed by the antenna and the FSS.

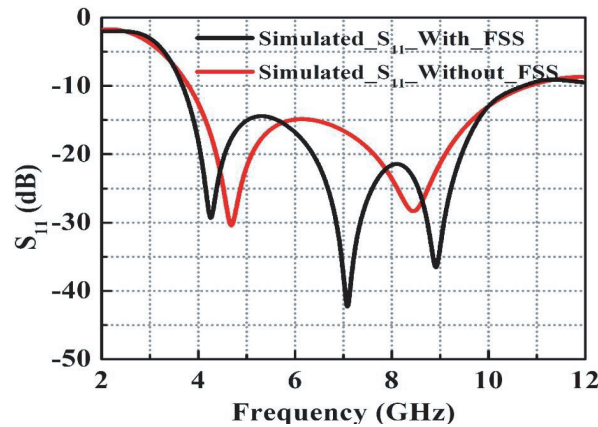


Figure 7. Simulated return loss performances of the antenna with and without the FSS.

The simulated directivities of the proposed antenna are plotted with and without FSS, and the results are tabulated in Fig. 8(a). The graph clearly explains the significant improvement in directivity with the addition of FSS. The simulated gains are plotted over 2–12 GHz with and without FSS and depicted in Fig. 8(b). Initially without FSS, the simulated peak gain was around 3 dBi at 11 GHz. Placing the FSS along with the above structure significantly improves the peak gain to 9.7 dBi at 10 GHz. The gain throughout UWB range is improved as well.

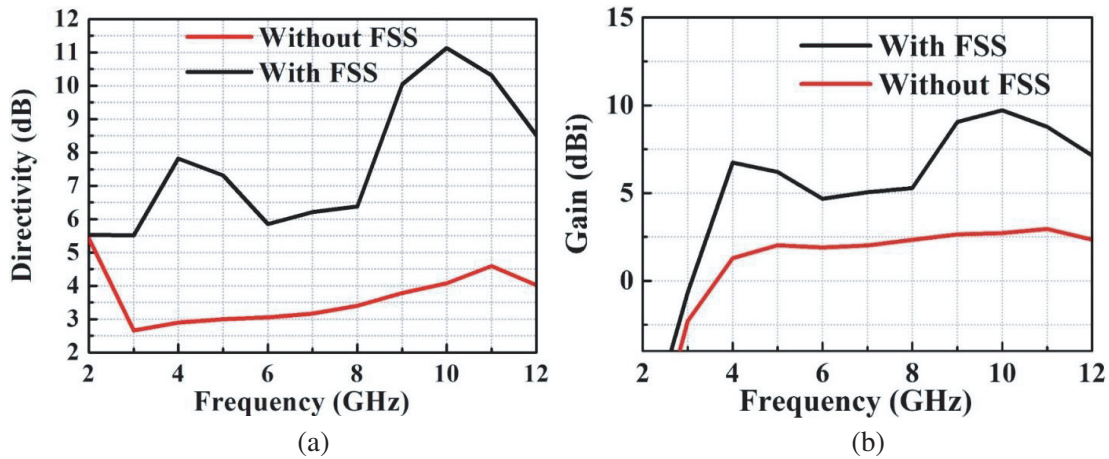


Figure 8. Simulated (a) directivity and (b) gain of the antenna with and without the FSS.

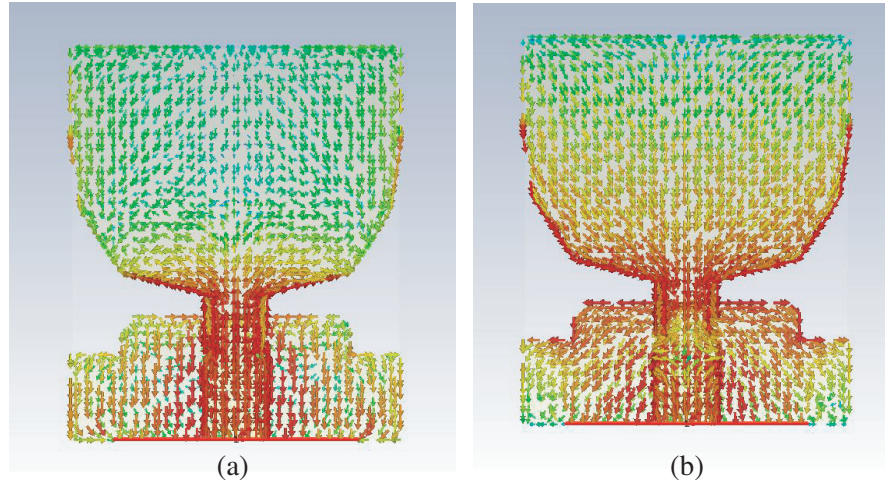


Figure 9. Simulated surface current distributions of the proposed antenna at (a) 4.6 GHz, and (b) 8.4 GHz.

After the addition of the proposed FSS with the antenna, the back radiated E-fields of the antenna are partially reflected by the single-layer FSS towards the antenna broadside direction. The electric field strength in the broadside direction of the antenna increases significantly due to the placement of FSS at a distance of 20 mm below the proposed antenna structure. The radiation reflected from the FSS constructively adds up with the radiation already radiating from the patch and the overall radiation in the broadside increases. This leads to the increase in antenna directivity towards the broadside direction. Hence, a considerable improvement in antenna gain is observed on the placement of the FSS. The surface current distributions of the antenna are plotted at 4.6 GHz and 8.4 GHz respectively as shown in Fig. 9. Result shows that the current is concentrated near the feed portion of the antenna, and the modified U-shape patch has less intensity than the feed. Thus, the feed portion is the short circuit, and the U-shaped portion represents the open circuit. Thus, the effective electrical length from the feed to the top of the U shape corresponds to $\lambda/4$. In the case of Fig. 9(b), the current is mainly concentrated in the edges of the U shape as well as in the ground plane. A null is visible in the centre of the feed portion. Thus, the effective electrical length of the antenna in this case is $\lambda/2$. Due to the concentration of current near the feed portion, the cross polarization of the antenna is much less improving the performance of the antenna. The radiation patterns of the proposed antenna with and without FSS are simulated. The radiating direction of the antenna is studied, and the co-polarization

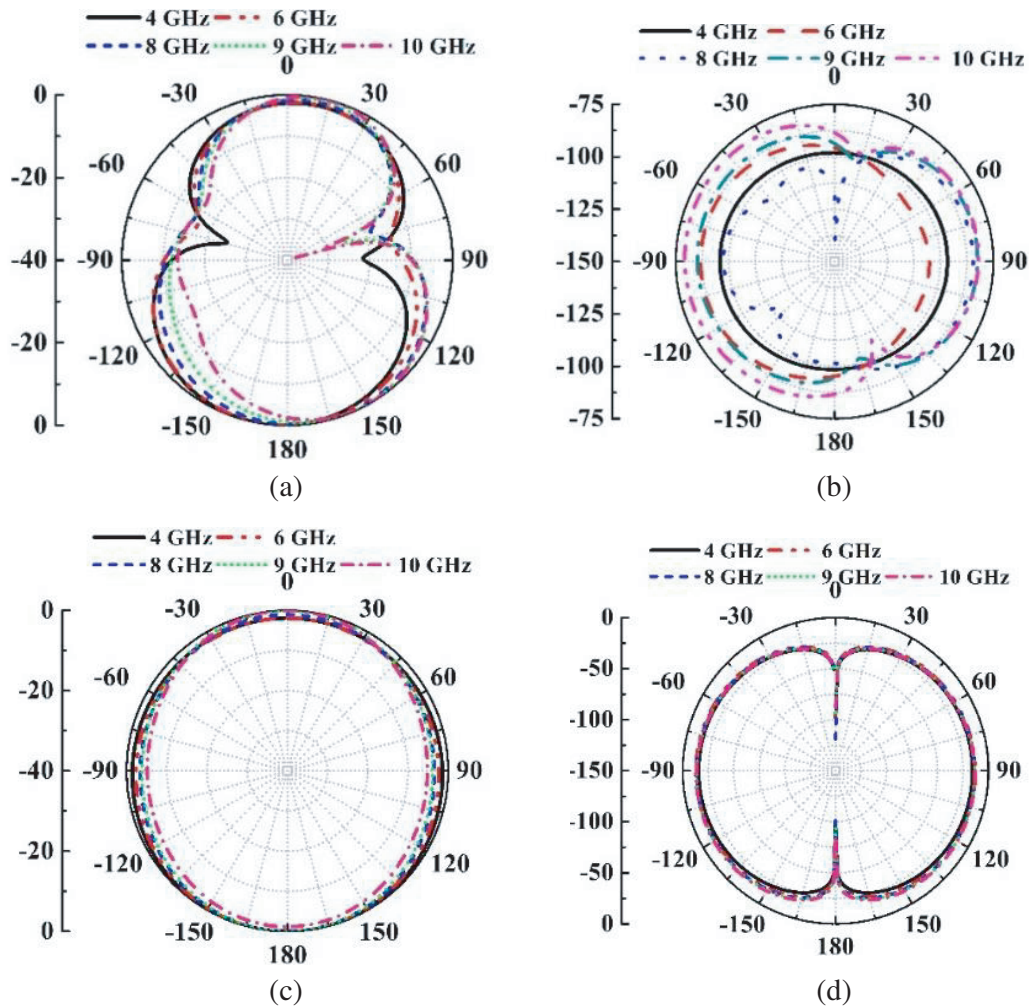


Figure 10. Simulated radiation patterns of the antenna without FSS at 4 GHz, 6 GHz, 8 GHz, 9 GHz and 10 GHz where (a) *E* plane co-polarization, (b) *E* plane cross-polarization, (c) *H*-plane co-polarization and (d) *H*-plane cross-polarization.

and cross-polarization of the antenna are plotted over the UWB range. The radiation patterns of the proposed antenna are plotted at 4 GHz, 6 GHz, 8 GHz, 9 GHz, and 10 GHz, with and without the FSS, as depicted in Fig. 10 and Fig. 11, respectively. In addition, radiation patterns at the starting point, middle point, and the end point frequencies of the UWB (3.6 GHz, 7.2 GHz and 10.8 GHz) are plotted in Fig. 12, for clarity.

4. EXPERIMENTAL VALIDATION

The prototypes of the proposed FSS and UWB patch antenna are fabricated using Monolithic Microwave Integrated Circuits (MMIC) process, and their various parameters are measured. An FR-4 substrate with dimensions of 16 mm \times 19 mm is used to print the antenna. The thickness of the substrate used is 1.6 mm. Modified U-shaped patch is printed on one side and most of the ground plane removed on the bottom side, leaving behind a partial ground plane. Front and back side photographs of the fabricated antenna are shown in Figs. 13(a) and (b), respectively. A 50 Ω SMA connector is soldered with the CPW feedline. Inner conductor of the SMA connector is soldered with the feed line, and the outer conductor is soldered with ground planes present on the back side of the antenna. A novel FSS of dimensions 52 mm \times 62.5 mm is etched on an FR-4 substrate and is placed behind the antenna at an

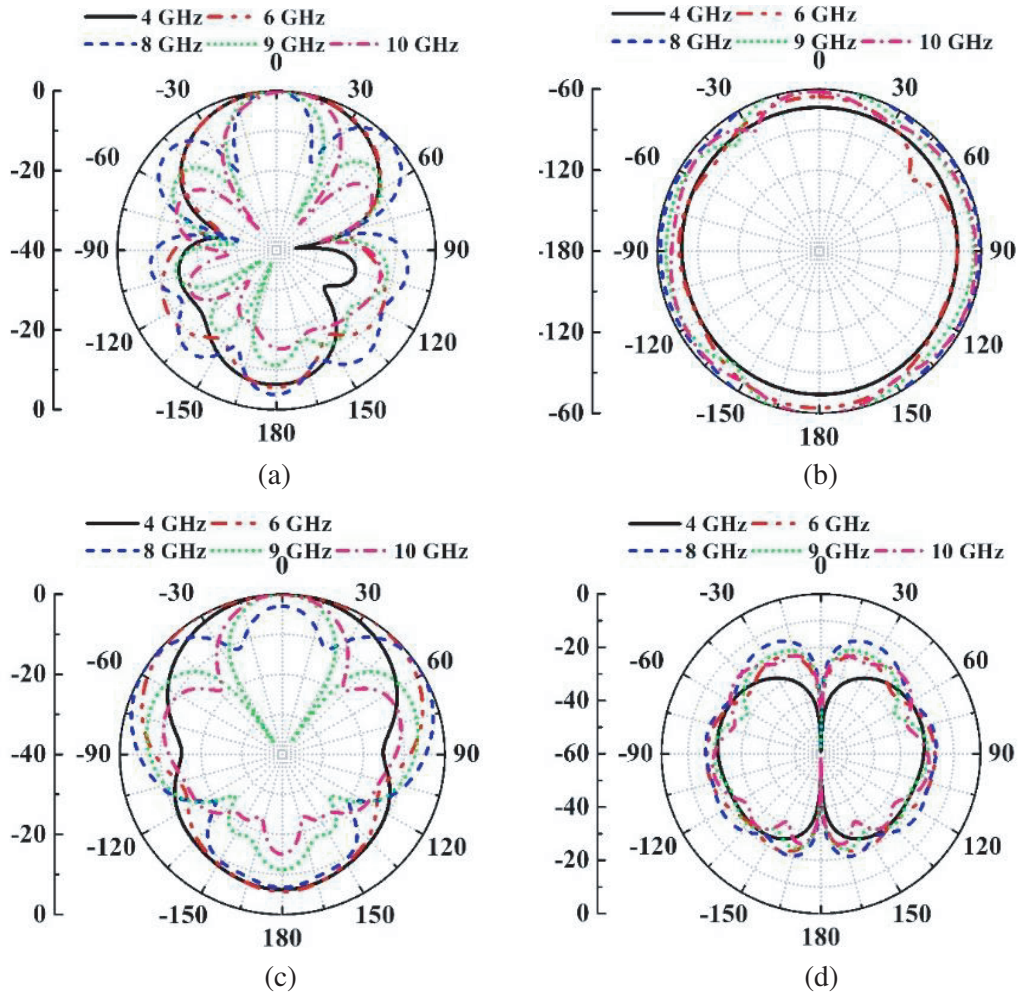


Figure 11. Simulated radiation patterns of the antenna with FSS at 4 GHz, 6 GHz, 8 GHz, 9 GHz and 10 GHz where (a) *E* Plane Co-Polarization, (b) *E* Plane cross-polarization, (c) *H*-Plane Co-Polarization and (d) *H*-Plane cross-polarization.

optimized distance of 20 mm. The proposed FSS structure is shown in Fig. 13(c). For measurement, the FSS structure is placed behind the antenna through a foam of thickness 20 mm, having the dimensions of the proposed novel FSS. Further, the foam provides a mechanical support to the antenna and helps in the easy measurement of the antenna with FSS. The complete arrangement of the antenna with the designed FSS with foam in between is described in Fig. 13(d).

S-parameter of the antenna is tested using the N5224B vector network analyzer (VNA) from Keysight. During the measurement, frequency sweep was set to 1 to 14 GHz with 1001 sample points. The transmission and reflection coefficient of the proposed FSS array was measured first, and then oblique angular stability was tested for 0° , 15° , 30° , 45° , 60° angles, as shown in Figs. 14(a)–(b), respectively. The proposed FSS is predominantly used as a reflector, and the proposed structure achieves a good angular stability. The obtained angular stability values prove that irrespective of the angle of the impinging wave, the FSS produces a stable reflected signal in the entire UWB region of operation. Measured S_{11} response of the antenna without FSS is shown in Fig. 15(a). The *S*-parameter of the antenna with FSS is also measured, and the results are plotted in Fig. 15(b). Result shows that measured reflection coefficient variation closely follows the simulated graph in both the cases. Small discrepancies between them are mostly attributed to the fabrication error and losses from the solder.

Gain of the UWB antenna was determined using gain transfer method. Initially, gain of the

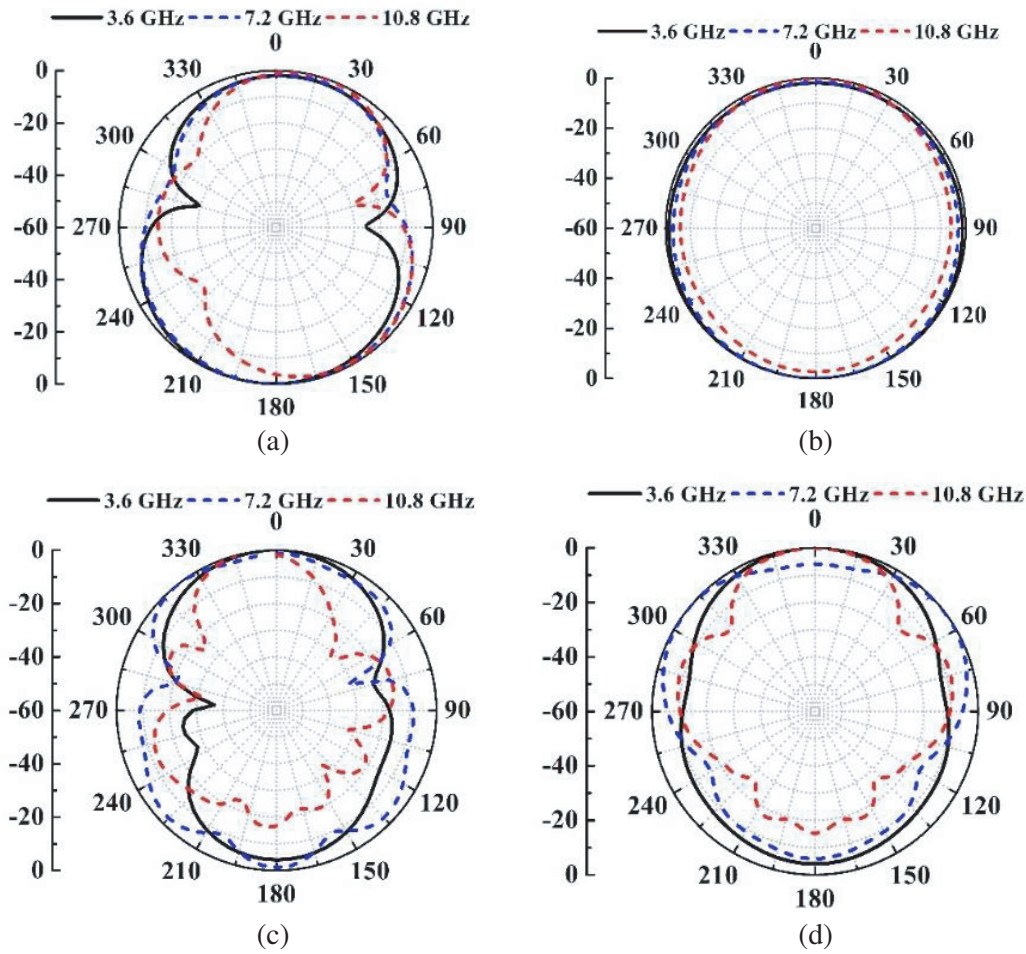


Figure 12. Simulated radiation patterns of the antenna at 3.6 GHz, 7.2 GHz and 10.8 GHz where (a) *E* Plane Co-Polarization, (b) *E* Plane cross-polarization, (c) *H*-Plane Co-Polarization and (d) *H*-Plane cross-polarization patterns.

standard horn antenna was noted from the available datasheet. Power fed to the transmitting horn was fixed at 10 dBm, and the distance between Tx horn and AUT was kept at 0.93 m. Tx horn is connected to a VNA with a 5.5 m long cable. Receiving antenna is connected to a Keysight signal analyzer N9020B to determine the peak power of the received signal. The power is found out at frequencies from 2 to 12 GHz. Initially, the AUT is replaced with a standard gain horn (SGH), and the received power is noted at the frequencies from 2 to 12 GHz. This is termed as P_{SGH} . By keeping the transmitting power and the distance between transmitter and receiver antennas unchanged, SGH at the receiver end is replaced with the UWB antenna (AUT), and the received power is noted at those frequencies again. It is denoted as P_{AUT} . Then gain of the patch antenna is obtained using the relation in Eq. (5) [54].

$$(G_{AUT})_{dB} = (G_{SGH})_{dB} + 10 \log_{10} \left(\frac{P_{AUT}}{P_{SGH}} \right) \tag{5}$$

The measured gain of the antenna with FSS is shown in Fig. 16. The measured gain is also compared with the simulated gain. It can be observed that the measured gain closely follows the simulated gain over the UWB range of operation.

Radiation characteristics of the UWB antenna are experimentally evaluated inside an anechoic chamber. Fig. 17 shows the detailed measurement setup inside the anechoic chamber. At the transmitting section, a broadband ridged horn antenna operating between 0.8 GHz and 18 GHz is kept. The UWB antenna whose radiation characteristics have to be determined acts as the antenna under

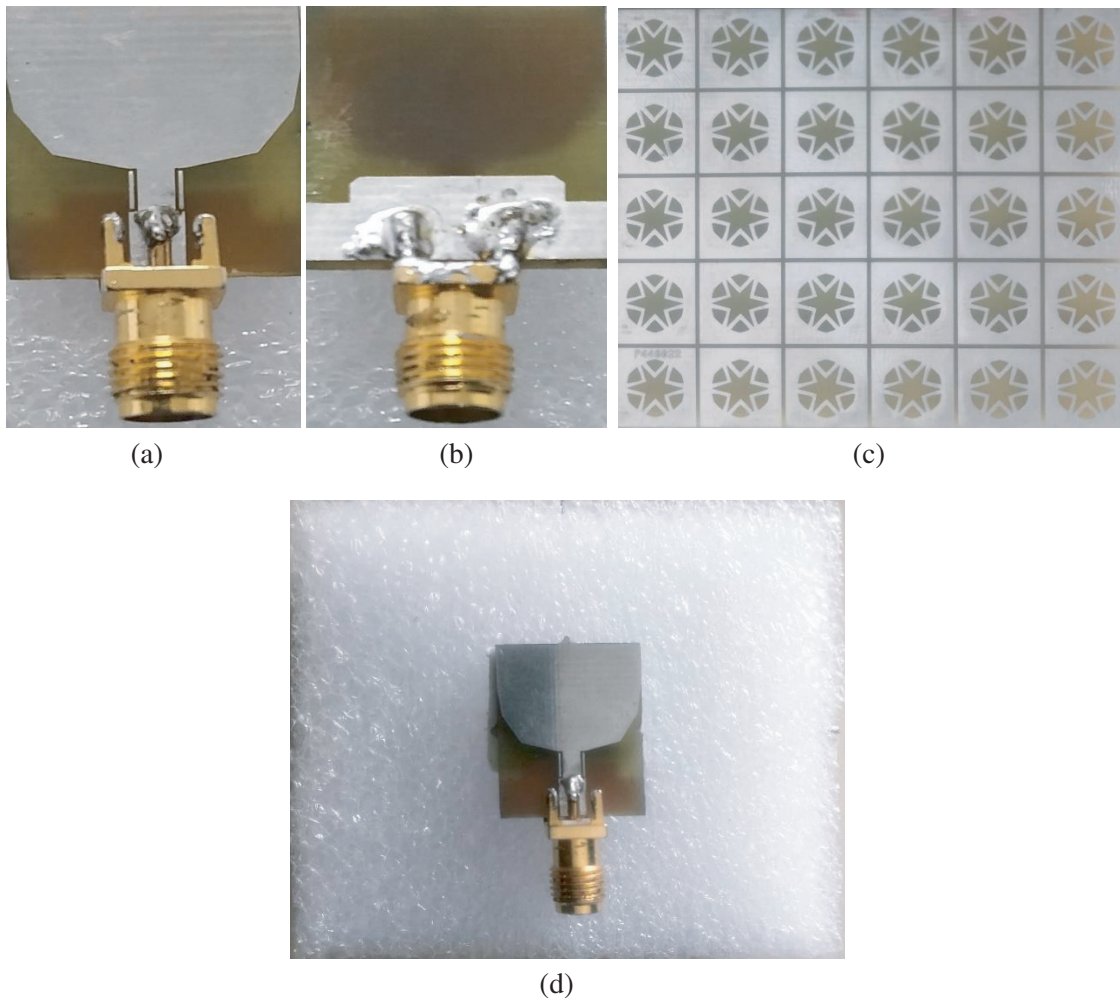


Figure 13. Photograph of the fabricated antenna where (a) top view and (b) bottom view, (c) fabricated FSS structure and (d) complete arrangement of the antenna with the FSS and foam in between them.

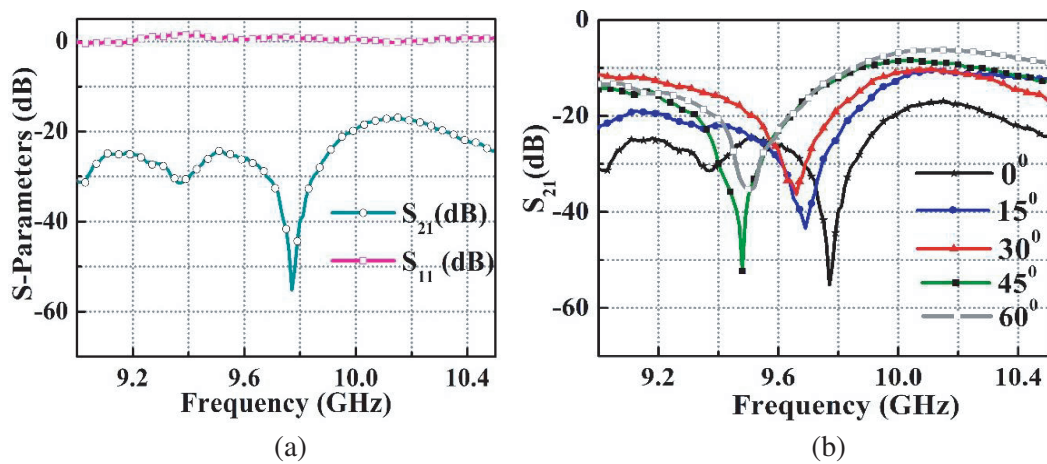


Figure 14. Measured (a) transmission, reflection coefficients and (b) angular stability at 0° , 15° , 30° , 45° , 60° oblique angles of the proposed FSS array.

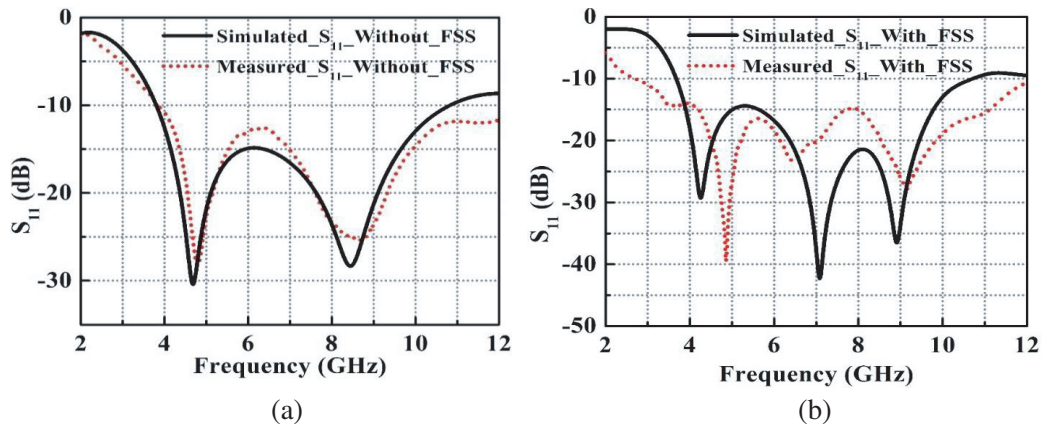


Figure 15. Simulated versus measured return loss of the (a) proposed antenna, and (b) antenna with FSS.

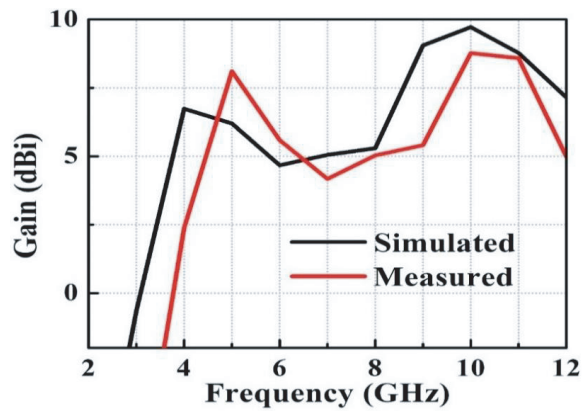


Figure 16. Simulated versus measured gain of the proposed antenna with FSS.

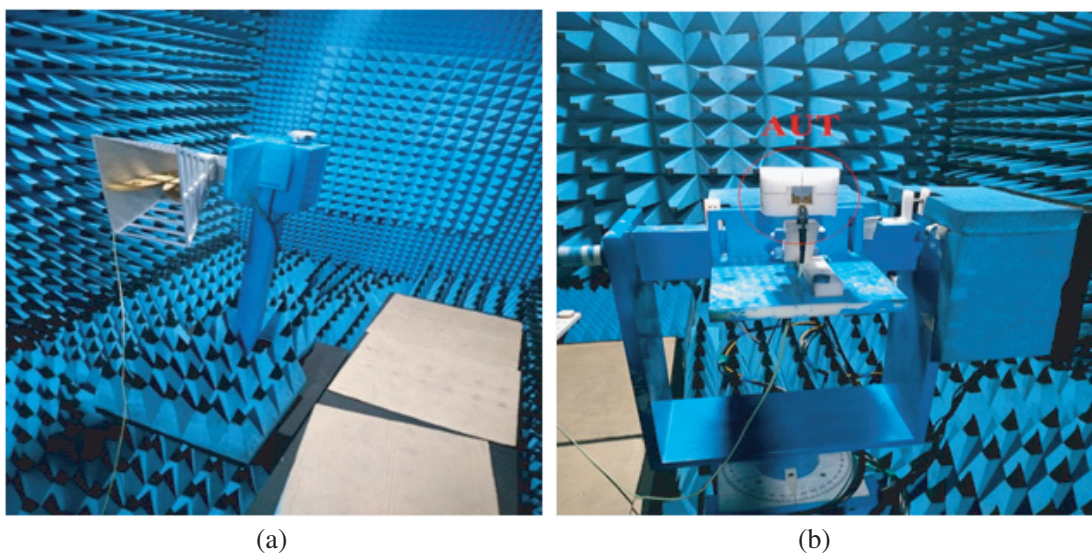


Figure 17. Radiation pattern measurement setup for the designed UWB antenna inside an Anechoic chamber where (a) Standard-gain transmitting horn antenna, and (b) UWB antenna at the receiving end.

test (AUT) at the receiving end. The antenna is mounted on a movable positioner system which has rotating features in three independent planes to fix its polarization and line of sight alignment with respect to transmitting horn. The distance between transmitting horn and AUT is fixed at 0.93 meters which satisfies the far-field condition at a distance greater than $2D^2/\lambda$. Here, D is the largest dimension among the transmitting and receiving antennas. For the given horn of $D = 34.4$ cm and lowest frequency of the sweep, far-field condition will be valid beyond the distance of 0.789 m. During the experiment inside the anechoic chamber, power to the transmitting horn antenna is kept as 10 dBm. Measured radiation patterns of the designed UWB antenna with FSS at 4 GHz, 6 GHz, 8 GHz, 9 GHz, and 10 GHz are shown in Fig. 18. For better understanding, the measured results are compared with the simulated ones for both E and H planes. In addition, the radiation pattern plots at the starting point, middle point, and the end point frequencies of the UWB (3.6 GHz, 7.2 GHz, and 10.8 GHz) are shown in Fig. 19. Results show a good agreement between the simulated and measured patterns for all frequencies. The performances of the antenna are compared with other state-of-the-art performances and tabulated in Table 2 for better clarity.

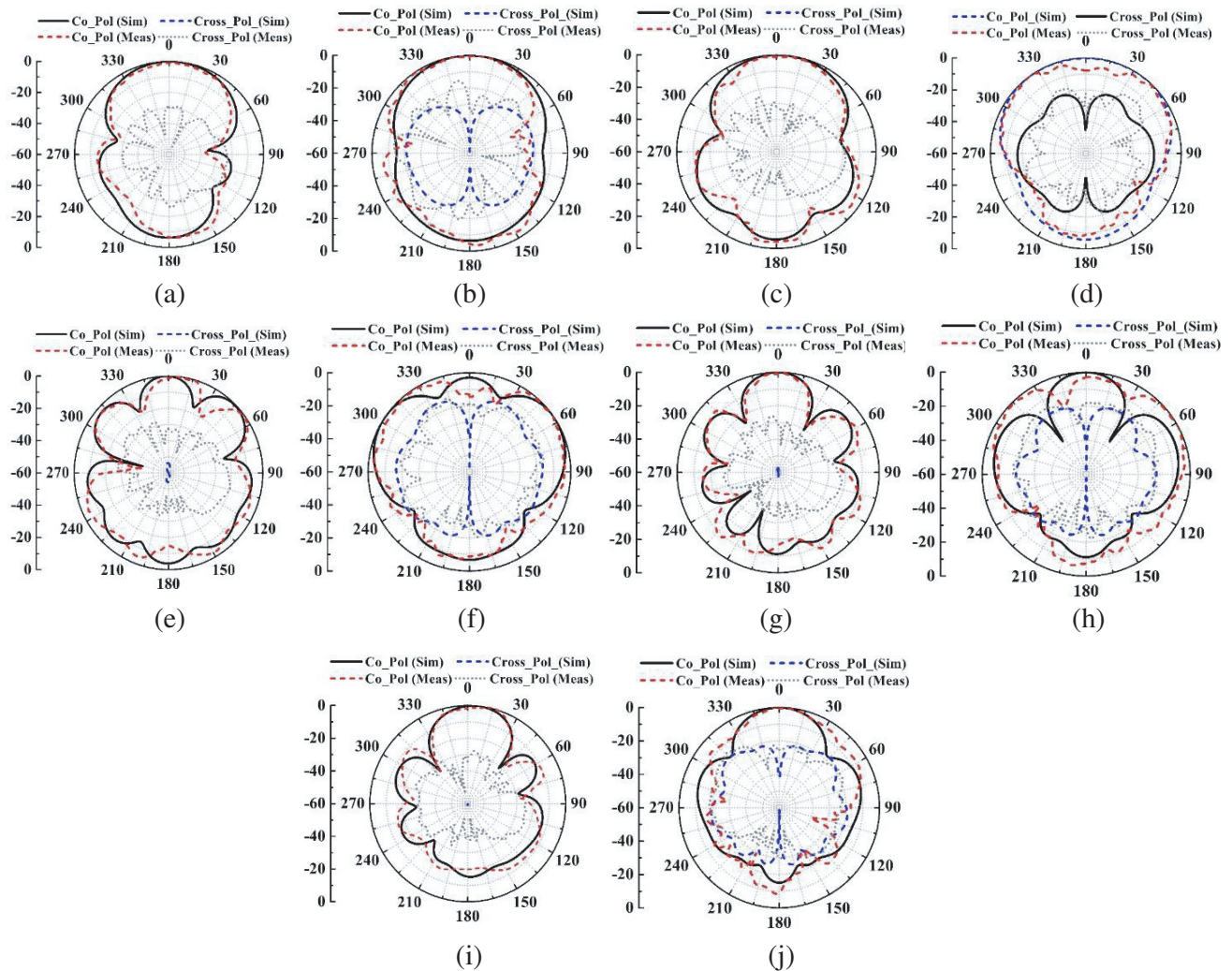


Figure 18. Simulated versus measured radiation patterns of the proposed antenna with FSS at various frequencies. The patterns (a), (c), (e), (g) and (i) presents the E plane radiation patterns and the patterns (b), (d), (f), (h) and (j) shows the H plane radiation patterns at 4 GHz, 6 GHz, 8 GHz, 9 GHz and 10 GHz, respectively.

Table 2. State-of-the-art performance comparison of the UWB antenna performances with other similar reported works.

Ref.	Size of the antenna (mm ²)	FSS unit cell size (mm ²)	Bandwidth (GHz)	No. of FSS Layers	Gain (Without FSS)	Gain (With FSS)	Gain Enhancement (dBi)	Approach
[13]	115 × 115	13.5 × 13.5	3–8	1	Around 6	Around 9.7	3.5–4	Dual polarized radiator mounted on a backing reflector
[15]	34 × 26	14 × 14	2.7–13.9	1	4.9	8.9	4	Compact unilayer FSS with UWB antenna.
[16]	35 × 30	10.8 × 10.8	3–13.4	2	2.5–5	5.5–8.5	2–4	Umbrella shaped UWB antenna with FSS as reflector
[17]	17.5 × 14.5	5.4 × 5.4	6.1–20.88	2	2–4	3.5–6.5	3	CPW fed printed UWB antenna with FSS
[27]	32 × 30	11 × 11	3.8–10.6	1	Around 5	Around 8.5	3.5	UWB antenna with FSS
[52]	32 × 32	-	3.1–10.6	-	1.7–4.2	-	-	Two open L shaped slots and narrow slots on the ground plane
[53]	24 × 28	-	2.91–11.4	-	NR	-	-	Y-shaped strips to annular ring
[54]	24.5 24.5	-	2.95–12.1	-	3.39	-	-	Asymmetrical rectangular patch with the U-shaped open-slot structure
[55]	Antenna 20 × 27 Antenna + FSS 84 × 84	14 × 14	4.7–14.9	1	4.2	8.7	4.3	Ultra wide stop band FSS
[56]	Antenna 63 × 63 Antenna + FSS 119 × 119	17 × 17	3–12	2	6	9.8	3.8	Multioctave FSS reflector
[57]	30 × 60	22.4 × 6.5	3.2–12	2	Around 5	Around 9	3–4	Slotted ground microstrip antenna with FSS reflector
This Work	Antenna (16 × 19) Antenna + FSS (52 × 62.5)	10.5 × 10.5	3.6–10.8	1	3	9.7	6.7	Modified U-shaped slot with Rectangular ground slot with a star shaped FSS structure.

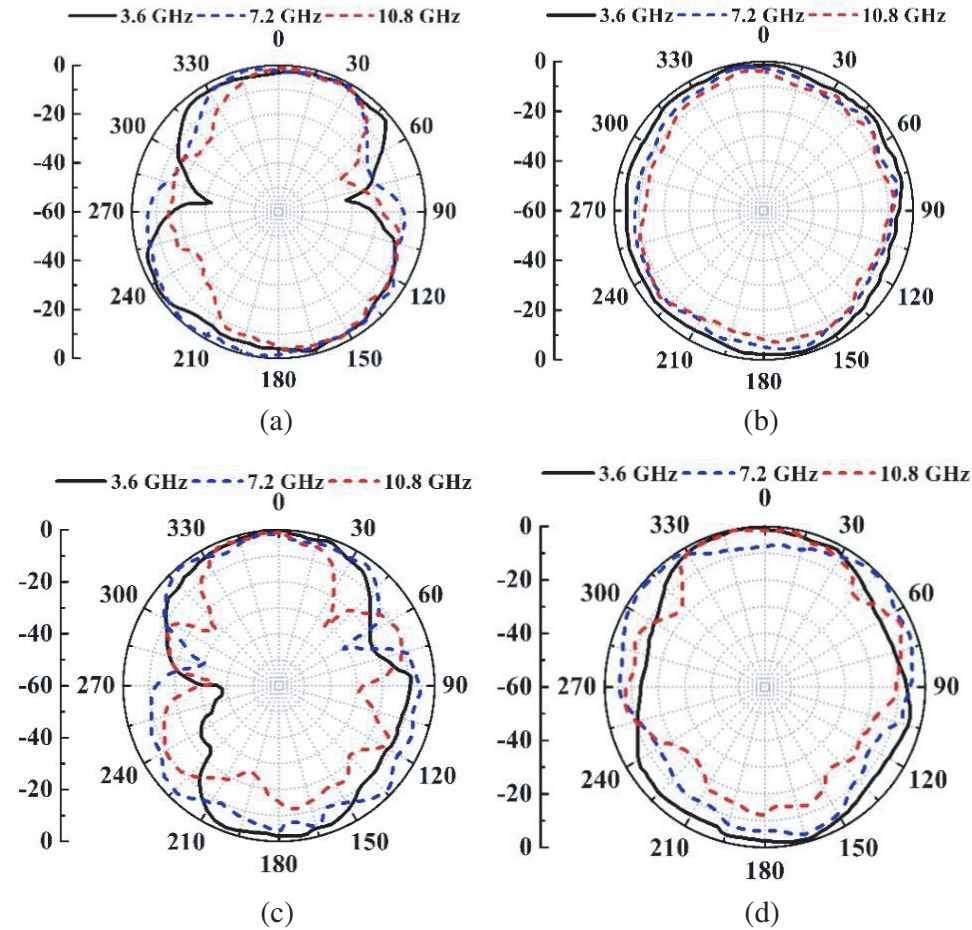


Figure 19. Measured radiation patterns of the antenna at 3.6 GHz, 7.2 GHz and 10.8 GHz where (a) *E* Plane Co-Polarization pattern, (b) *E* Plane cross-polarization pattern, (c) *H*-Plane Co-Polarization pattern and (d) *H*-Plane cross-polarization pattern.

5. CONCLUSION

In this paper, a single element UWB microstrip patch antenna with high directivity is designed and measured. A single layer FSS with good angular stability is proposed. All the parameters of the designed FSS are studied, measured, and presented systematically. The antenna designed as a monopole antenna with impedance bandwidth from 3.6 to 10.8 GHz. The addition of the FSS augments the gain, and an improvement of 6.7 dBi at 10 GHz is attained as compared to the stand-alone antenna. The antenna is fabricated, and the performance characteristics are verified by measurements. All measured responses are verified with full-wave and circuit simulations up to a reasonable extent. The total volume of the proposed structure is very low which can be utilized for wireless communication applications, GPRs, microwave imaging, etc.

REFERENCES

1. Aiello, G. R. and G. D. Rogerson, "Ultra-wideband wireless systems," *IEEE Microw. Mag.*, Vol. 4, No. 2, 36–47, 2003.
2. Chung, K. L., W. Y. Tam, and H. K. Kan, "A compact wideband PIFA," *Microwave and Optical Technology Letters*, Vol. 51, 2554–2556, November 2009.

3. Siwiak, K. and D. McKeown, *Ultra-Wideband Radio Technology*, No. 9, 193, John Wiley & Sons, Ltd, Chichester, UK, 2004.
4. Ranga, Y., L. Matekovits, K. P. Esselle, and A. R. Weily, "Multioctave frequency selective surface reflector for ultrawideband antennas," *IEEE Antennas and Wireless Propagation Letters*, Vol. 10, 219–222, 2011.
5. Kumar, C., M. I. Pasha, and D. Guha, "Defected ground structure integrated microstrip array antenna for improved radiation properties," *IEEE Antennas and Wireless Propagation Letters*, Vol. 16, 310–312, 2017.
6. Xue, K., H. Zhai, S. Li, and Y. Shang, "A miniaturized absorber frequency selective surface with good angular stability," *IEEE Antennas and Wireless Propagation Letters*, Vol. 19, No. 1, 24–28, 2020.
7. Mirza, H., T. M. Hossain, P. J. Soh, et al., "Deployable linear-to-circular polarizer using PDMS based on unloaded and loaded circular FSS arrays for pico-satellites," *IEEE Access*, Vol. 7, 2034–2041, 2019.
8. Syed, I. S., Y. Ranga, L. Matekovits, K. P. Esselle, and S. G. Hay, "A singlelayer frequency-selective surface for ultrawideband electromagnetic shielding," *IEEE Trans. Electromagn. Compat.*, Vol. 56, No. 6, 1404–1411, 2014.
9. Lazaro, A., A. Ramos, D. Girbau, and R. Villarino, "A novel UWB RFID tag using active frequency selective surface," *IEEE Transactions on Antennas and Propagation*, Vol. 61, No. 3, 1155–1165, 2013.
10. Sheng, X., J. Ge, K. Han, and X. Zhu, "Transmissive/reflective frequency selective surface for satellite applications," *IEEE Antennas and Wireless Propagation Letters*, Vol. 17, No. 7, 1136–1140, 2018.
11. Chatterjee, A. and S. K. Parui, "Performance enhancement of a dualband monopole antenna by using a frequency-selective surfacebased corner reflector," *IEEE Transactions on Antennas and Propagation*, Vol. 64, No. 6, 2165–2171, 2016.
12. Kushwaha, N., R. Kumar, R. V. S. Ram Krishna, and T. Oli, "Design and analysis of new compact UWB frequency selective surface and its equivalent circuit," *Progress In Electromagnetics Research*, Vol. 46, 31–39, 2014.
13. Yahya, R., A. Nakamura, M. Itami, and T. A. Denidni, "A novel UWB FSS-based polarization diversity antenna," *IEEE Antennas and Wireless Propagation Letters*, Vol. 16, 2525–2528, 2017.
14. Hua, B., X. He, and Y. Yang, "Polarisation-independent UWB frequency selective surface based on 2.5 D miniaturised hexagonal ring," *Electronics Letters*, Vol. 53, No. 23, 1502–1504, 2017.
15. Tahir, F. A., T. Arshad, S. Ullah, and J. A. Flint, "A novel FSS for gain enhancement of printed antennas in UWB frequency spectrum," *Microwave and Optical Technology Letters*, Vol. 59, No. 10, 2698–2704, 2017.
16. Kundu, S., A. Chatterjee, S. K. Jana, and S. K. Parui, "A compact umbrella-shaped UWB antenna with gain augmentation using frequency selective surface," *Radioengineering*, Vol. 27, No. 2, 448–454, 2018.
17. Kundu, S., "Gain augmentation of a CPW fed printed miniature UWB antenna using frequency selective surface," *Microw. Opt. Technol. Lett.*, Vol. 60, No. 7, 1820–1826, 2018.
18. Mondal, R., P. S. Reddy, D. C. Sarkar, and P. P. Sarkar, "Compact ultrawideband antenna: Improvement of gain and FBR across the entire bandwidth using FSS," *IET Microw. Antennas Propag.*, Vol. 14, No. 1, 66–74, 2019.
19. Das, P. and K. Mandal, "Modelling of ultra-wide stop-band frequency-selective surface to enhance the gain of a UWB antenna," *IET Microw. Antennas Propag.*, Vol. 13, No. 3, 269–277, 2019.
20. Buynevich, V., H. M. Jol, and D. M. F. Gerald, "Coastal environments," *Ground Penetrating Radar: Theory and Applications*, 299–322, 1st Edition, Jol H. M. (ed.), Elsevier Press, 2009.
21. Cheng, H., H. Yang, Y. Li, and Y. Chen, "A compact Vivaldi antenna with artificial material lens and sidelobe suppressor for GPR applications," *IEEE Access*, Vol. 8, 64056–64063, 2020.

22. Yektakhah, B., J. Chiu, F. Alsallum, and K. L.-P. Sarabandi, "Low-frequency, UWB antenna for imaging of deeply buried targets," *IEEE Geosci. Remote Sens. Lett.*, Vol. 17, No. 7, 1168–1172, 2019.
23. Guo, J., J. Tong, Q. Zhao, J. Jiao, J. Huo, and C. Ma, "An ultrawide band antipodal Vivaldi antenna for airborne GPR application," *IEEE Geosci. Remote Sens. Lett.*, Vol. 16, No. 10, 1560–1564, 2019.
24. Guo, L., H. Yang, Q. Zhang, and M. Deng, "A compact antipodal tapered slot antenna with artificial material lens and reflector for GPR applications," *IEEE Access*, Vol. 6, 44244–44251, 2018.
25. Mahmud, M. Z., M. T. Islam, N. Misran, S. Kibria, and M. Samsuzzaman, "Microwave imaging for breast tumor detection using uniplanar AMC based CPW-fed microstrip antenna," *IEEE Access*, Vol. 6, 44763–44775, 2018.
26. Islam, M. T., M. M. Islam, M. Samsuzzaman, M. R. I. Faruque, and N. Misran, "A negative index metamaterial-inspired UWB antenna with an integration of complementary SRR and CLS unit cells for microwave imaging sensor applications," *Sensors*, Vol. 15, No. 5, 11601–11627, 2015.
27. Abdulhasan, R. A., R. Alias, K. N. Ramli, F. C. Seman, and R. A. Abd-Alhameed, "High gain CPW-fed UWB planar monopole antenna-based compact uniplanar frequency selective surface for microwave imaging," *Int. J. RF Microw. Comput. Aided Eng.*, Vol. 29, No. 8, e21757, 2019.
28. Lin, C. C., Y. C. Kan, L. C. Kuo, and H. R. Chuang, "A planar triangular monopole antenna for UWB communication," *IEEE Microwave and Wireless Components Letters*, Vol. 15, No. 10, 624–626, 2005.
29. Deng, C., Y. Xie, and P. Li, "CPW-fed planar printed monopole antenna with impedance bandwidth enhanced," *IEEE Antennas and Wireless Propagation Letters*, Vol. 8, 1394–1397, 2009.
30. Liu, J., S. Zhong, and K. P. Esselle, "A printed elliptical monopole antenna with modified feeding structure for bandwidth enhancement," *IEEE Transactions on Antennas and Propagation*, Vol. 59, No. 2, 667–670, 2011.
31. Abbosh, A. M. and M. E. Bialkowski, "Design of ultrawideband planar monopole antennas of circular and elliptical shape," *IEEE Transactions on Antennas and Propagation*, Vol. 56, No. 1, 17–23, 2008.
32. Liang, J., C. C. Chiau, X. Chen, et al., "Printed circular disc monopole antenna for ultra-wideband applications," *Electronics Letters*, Vol. 40, No. 20, 1246–1247, 2004.
33. Gopikrishna, M., D. D. Krishna, C. K. Anandan, et al., "Design of a compact semi-elliptic monopole slot antenna for UWB systems," *IEEE Transactions on Antennas and Propagation*, Vol. 57, No. 6, 1834–1837, 2009.
34. Alsath, M. G. N. and M. Kanagasabai, "Compact UWB monopole antenna for automotive communications," *IEEE Transactions on Antennas and Propagation*, Vol. 63, No. 9, 4204–4208, 2015.
35. Hong, C. Y., C. W. Ling, I. Y. Tarn, et al., "Design of a planar ultrawideband antenna with a new band-notch structure," *IEEE Transactions on Antennas and Propagation*, Vol. 55, No. 12, 3391–3397, 2007.
36. Lu, Y., Y. Huang, H. T. Chattha, et al., "Reducing ground-plane effects on UWB monopole antennas," *IEEE Antennas and Wireless Propagation Letters*, Vol. 10, 147–150, 2011.
37. Ren, J., W. Hu, Y. Yin, and R. Fan, "Compact printed MIMO antenna for UWB applications," *IEEE Antennas and Wireless Propagation Letters*, Vol. 29, No. 13, 1517–1520, 2014.
38. Zhou, Z. L., L. Li, and J. S. Hong, "Compact UWB printed monopole antenna with dual narrow band notches for WiMAX/WLAN bands," *Electronics Letters*, Vol. 47, No. 20, 1111–1112, September 29, 2011.
39. Liu, W., Y. Yin, W. Xu, and S. Zuo, "Compact open-slot antenna with bandwidth enhancement," *IEEE Antennas and Wireless Propagation Letters*, Vol. 18, No. 10, 850–853, 2011.
40. Lu, Y., Y. Huang, Y. C. Shen, and H. T. Chattha, "A further study of planar UWB monopole antennas," *Proc. Loughbrough Antennas Propag. Conf. 2007*, 353–356, September 2009.

41. Chan, K. C. L., Y. Huang, and X. Zhu, "A planar elliptical monopole antenna for UWB applications," *Proc. IEEE/ACES Int. Conf. Wireless Commun. Appl. Comput. Electromagn.*, 182–185, April 2005.
42. Chen, Z. N., M. J. Ammann, X. Qing, X. H. Wu, T. S. P. See, and A. Cat, "Planar antennas," *IEEE Microw. Mag.*, Vol. 7, No. 6, 63–73, December 2006.
43. Liang, J. X., C. C. Chian, X. D. Chen, and C. G. Parini, "Study of a printed circular disc monopole antenna for UWB systems," *IEEE Transactions on Antennas and Propagation*, Vol. 53, No. 11, 3500–3504, November 2005.
44. Bekasiewicz, A. and S. Koziel, "Structure and computationally efficient simulation-driven design of compact UWB monopole antenna," *IEEE Antennas and Wireless Propagation Letters*, Vol. 14, 1282–1285, 2015.
45. Fereidoony, F., S. Chamaani, and S. A. Mirtaheri, "UWB monopole antenna with stable radiation pattern and low transient distortion," *IEEE Antennas and Wireless Propagation Letters*, Vol. 10, 302–305, 2011.
46. Pandey, G. K., H. S. Singh, P. K. Bharti, et al., "UWB monopole antenna with enhanced gain and stable radiation pattern using gate like structures." *Int. Conf. Microwave Photonics, ICMAP*, 4–7, Dhanbad, India, December 2013.
47. Ryu, K. S. and A. A. Kishk, "UWB dielectric resonator antenna having consistent omnidirectional pattern and low cross-polarization characteristics," *IEEE Transactions on Antennas and Propagation*, Vol. 59, No. 4, 1403–1408, 2011.
48. Wang, J. and Y. Yin, "Differential-fed UWB microstrip antenna with improved radiation patterns," *Electronics Letters*, Vol. 50, No. 20, 1412–1414, 2014.
49. Hsieh, T. H. and C. S. Lee, "Double-layer high-gain microstrip array antenna," *IEEE Transactions on Antennas and Propagation*, Vol. 48, No. 7, 1033–1035, 2000.
50. Moharamzadeh, E. and A. M. Javan, "Triple-band frequency-selective surfaces to enhance gain of x-band triangle slot antenna," *IEEE Antennas and Wireless Propagation Letters*, Vol. 12, 1145–1148, 2013.
51. Das, P. and K. Mandal, "Modelling of ultra-wide stop-band frequency-selective surface to enhance the gain of a UWB antenna," *IET Microwaves, Antennas & Propagation*, Vol. 13, No. 3, 269–277, 2018.
52. Ranga, Y., L. Matekovits, K. P. Esselle, and A. R. Weily, "Multioctave frequency selective surface reflector for ultrawideband antennas," *IEEE Antennas and Wireless Propagation Letters*, Vol. 10, 219–222, 2011.
53. Krishna, R. V. S. and R. Kumar, "Slotted ground microstrip antenna with FSS reflector for high-gain horizontal polarisation," *Electronics Letters*, Vol. 51, No. 8, 599–600, 2015.
54. Al-Ghuri, A. J. A., I. B. M. Ibrahim, M. Y. Zeain, and Z. Zakaria, "Compact size and high gain of CPW-fed UWB strawberry artistic shaped printed monopole antennas using FSS single layer reflector," *IEEE Access*, Vol. 8, 92697–92707, 2020.
55. Paul, G. S. and K. Mandal, "Polarization-insensitive and angularly stable compact ultrawide stop-band frequency selective surface," *IEEE Antennas and Wireless Propagation Letters*, Vol. 18, No. 9, 1917–1921, 2019.
56. Hong, T., M. Wang, K. Peng, Q. Zhao, and S. Gong, "Compact ultra-wide band frequency selective surface with high selectivity," *IEEE Transactions on Antennas and Propagation*, Vol. 68, No. 7, 5724–5729, 2020.
57. Sampath, S. S. and R. Sivasamy, "A single-layer UWB frequency-selective surface with band-stop response," *IEEE Transactions on Electromagnetic Compatibility*, Vol. 62, No. 1, 276–279, 2018.